Author Manuscript

ADAM10-mediated ephrin-B2 shedding promotes myofibroblast activation and organ fibrosis

David Lagares[1,8,*], **Parisa Ghassemi-Kakroodi**[2,8], **Caroline Tremblay**[2], **Alba Santos**[1], **Clemens K. Probst**[1], **Alicia Franklin**[1], **Daniela M. Santos**[1], **Paula Grasberger**[1], **Neil Ahluwalia**[1], **Sydney B. Montesi**[1], **Barry S. Shea**[1], **Katharine E. Black**[1], **Rachel Knipe**[1], **Meryem Blati**[2], **Murray Baron**[3], **Brian Wu**[4], **Hassan Fahmi**[2], **Rajiv Gandhi**[4], **Annie Pardo**[5], **Moisés Selman**[6], **Jiangping Wu**[2], **Jean-Pierre Pelletier**[2], **Johanne Martel-Pelletier**[2], **Andrew M. Tager**[1,9,*], and **Mohit Kapoor**[2,4,7,9,*]

[1]Division of Pulmonary and Critical Care Medicine, Fibrosis Research Center and Center for Immunology and Inflammatory Diseases, Department of Medicine, Massachusetts General Hospital, Harvard Medical School, Massachusetts, USA

[2]Faculty of Medicine, University of Montreal Research Centre (CRCHUM), Quebec, Montreal, Canada

[3]Division of Rheumatology, Jewish General Hospital, McGill University, Montreal, Canada

[4]The Arthritis Program, University Health Network, Toronto Ontario, Canada

[5]Facultad de Ciencias, Universidad Nacional Autonoma de Mexico, Mexico City, Mexico

[6]Instituto Nacional de Enfermedades Respiratorias "Ismael Cosio Villegas", Mexico City, Mexico

[7]Division of Genetics and Development, Krembil Research Institute, University Health Network and Department of Surgery and Department of Laboratory Medicine and Pathobiology, University of Toronto, Toronto, Ontario, Canada

Abstract

*Correspondence should be addressed to: Dr. Mohit Kapoor, Division of Genetics and Development, Krembil Research Institute, University Health Network and Department of Surgery, University of Toronto, 60 Leonard Avenue, Toronto Ontario, Canada M5T 2S8. mkapoor@uhnresearch.ca Or Dr. David Lagares, Division of Pulmonary and Critical Care Medicine and Fibrosis Research Center, Department of Medicine, Massachusetts General Hospital, Harvard Medical School, Massachusetts, USA.dlagares@mgh.harvard.edu.

[8]These authors contributed equally to this work.

[9]These authors contributed equally to this work.

Maladaptive wound healing responses to chronic tissue injury result in organ fibrosis. Fibrosis, which entails excessive extracellular matrix (ECM) deposition and tissue remodelling by activated myofibroblasts, leads to loss of proper tissue architecture and organ function; however the molecular mediators of myofibroblast activation remain to be fully identified. Here we identify soluble ephrin-B2 as a novel pro-fibrotic mediator in lung and skin fibrosis. We provide molecular, functional and translational evidence that the ectodomain of membrane-bound ephrin-B2 is shed from fibroblasts into the alveolar airspace after lung injury. Shedding of soluble ephrin-B2 (sEphrin-B2) promotes fibroblast chemotaxis and activation via EphB3/EphB4 receptor signaling. We found that mice lacking ephrin-B2 in fibroblasts are protected from skin and lung fibrosis and that a distintegrin and metalloproteinase 10 (ADAM10) is the major ephrin-B2 sheddase in fibroblasts. ADAM10 is induced by transforming growth factor-β1 (TGF-β1), and ADAM10-mediated sEphrin-B2 generation is required for TGF-β1–induced myofibroblast activation. Pharmacological inhibition of ADAM10 reduces sEphrin-B2 levels in bronchoalveolar lavage and prevents lung fibrosis in mice. Consistent with the mouse data, ADAM10/sEphrin-B2 signaling is upregulated in fibroblasts from human subjects with idiopathic pulmonary fibrosis. These results uncover a new molecular mechanism of tissue fibrogenesis and identify sEphrin-B2, its receptors Eph3/Eph4, and ADAM10 as potential therapeutic targets in the treatment of fibrotic diseases.

Introduction

Dysregulated wound repair processes can lead to the development of tissue fibrosis in most organs. Fibrosis is characterized by excess accumulation of collagens and other matrix proteins that result in the distortion of tissue architecture, and ultimately organ failure, in a variety of human diseases including idiopathic pulmonary fibrosis and systemic sclerosis (SSc, scleroderma)[1]. This pathological matrix protein accumulation is attributable to the excess recruitment of fibroblasts to sites of tissue injury, and/or their excessive activation to an effector myofibroblast phenotype[1-5]. We have previously found increased expression of genes associated with cell migration and myofibroblast activation in the lungs of individuals with IPF with a more rapidly advancing clinical course, leading us to hypothesize that this set of genes contributes to IPF progression[6]. If so, then elucidating the regulation of fibroblast migration and activation will not only further enhance our understanding of the pathogenesis of fibrosis, but also provide targets for novel anti-fibrotic therapies.

To identify putative genes that regulate profibrotic fibroblast functions, we analyzed a publicly available microarray data set comparing the gene expression of lung fibroblasts isolated from individuals with IPF or SSc-associated interstitial lung disease (SSc-ILD) to that of control lung fibroblasts[7]. Among genes upregulated in fibroblasts from both individuals with IPF and SSc-ILD in this data set we found *Efnb2* (Gene Expression Omnibus accession number GSE1724, *Efnb2* probe: 34334_at)[7]. *Efnb2* encodes the transmembrane protein ephrin-B2, which belongs to the family of ephrin ligands and has previously been described to exhibit pro-migratory activities[8,9]. Ephrins are glycosyl-phosphatidylinositol-linked (ephrin-A1-6) and transmembrane (ephrin-B1-3) cell surface ligands that bind to Eph receptors at the surface of adjacent cells. This interaction initiates bi-directional signaling events between the receptor-expressing (forward signaling) and ligand-expressing (reverse signaling) cells[10]. Ephrin/Eph signaling controls tissue patterning

and cell motility during embryonic development[11]. Consistent with its pro-migratory activities, ephrin-B2 ligand, which signals through EphB receptors, also controls cell motility and adhesion during assembly of the blood vessel wall[9,12,13]. Genetic inactivation of the *Efnb2* gene in smooth muscle cells and pericytes during development results in disrupted microvessel architecture and increased vascular permeability[9]. Mice lacking the intracellular PDZ signaling domain of ephrin-B2, which consequently attenuates ephrin-B2 reverse signaling, have compromised vascular stabilization by pericytes, resulting in increased capillary rarefaction and fibrosis after kidney injury in mice[14]. In human disease, ephrin-B2 expression is increased in small vessels and in vascular smooth muscle in clinically-involved skin of individuals with systemic sclerosis[15]. While ephrin-B2 signaling has been implicated in vascular contributions to the development of fibrosis in mouse models and human disease, the full spectrum of cellular and molecular mechanisms through which ephrin-B2 signaling may contribute to the development of tissue fibrosis has not been investigated. Here we describe a novel mechanism by which ADAM10-mediated proteolytic shedding of ephrin-B2's ectodomain, here-in referred to as soluble ephrin-B2 (sEphrin-B2), promotes fibroblast recruitment and activation. We provide molecular, genetic, functional and translational evidence that this mechanism plays an important role in fibroblast activation *in vitro* and in the development of the lung and skin fibrosis *in vivo*.

Results

Bleomycin-induced lung fibrosis requires fibroblast ephrin-B2

Our initial studies confirmed that expression of ephrin-B2, but not other members of the ephrin family of ligands, is markedly higher in lung fibroblasts isolated from individuals with IPF compared with those from lung tissue from control subjects, as demonstrated by mRNA and protein analyses (Fig. 1a,b). We then investigated whether fibroblast ephrin-B2 is required for the development of fibrosis *in vivo*. Since mice that are globally ephrin-B2-deficient die at mid-gestation due to defective cardiovascular development[13,16], we generated mice in which we could conditionally delete *Efnb2* in collagen-expressing cells such as fibroblasts. We crossed mice with *Efnb2* flanked by loxP sites (*Efnb2^loxP/loxP* mice)[17] to mice that express a tamoxifen-inducible Cre recombinase driven by the mouse *Col1a2* (collagen, type I, alpha 2) promoter (*Col1a2-Cre/ERT* mice) (Fig. 1c). Tamoxifen treatment of offspring that were homozygous for the "floxed" *Efnb2* allele and hemizygous for the *Col1a2-Cre* transgene (*Efnb2^loxP/loxP*; *Col1a2-Cre/ERT* mice), as confirmed by PCR (Fig. 1d), led to the deletion of the *Efnb2* gene in fibroblasts and the generation of *Efnb2* conditional knockout mice, here-inreferredto as *ephrinb2*-CKO mice. Littermates treated with corn oil vehicle alone were used as controls, here-in referred to as *ephrinb2*-C mice. Western blotting forephrin-B2 protein demonstrated markedly lower expression in extracts from lung fibroblasts of *ephrinb2*-CKO mice compared to *ephrinb2*-C mice. We observed preservation of ephrin-B2 protein in extracts from alveolar macrophages in *ephrinb2*-CKO mice compared to *ephrinb2*-C mice (Fig. 1e). We also isolated alveolar epithelial cells from *ephrinb2*-C and *ephrinb2*-CKO mice, but we did not observe ephrin-B2 protein expression by Western blotting in these cells from *ephrinb2*-C mice, and thus we could not compare its potential preservation in alveolar epithelial cells from *ephrinb2*-CKO mice.

Ephrinb2-CKO and *ephrinb2*-C mice were then challenged with intratracheal bleomycin or PBS (Fig. 1f). Blinded histological analysis revealed that lung parenchymal fibrosis observed in *ephrinb2*-Cat 14d post-bleomycin challenge was markedly lower in *ephrinb2*-CKO mice, which was associated with substantially lower lung hydroxyproline (collagen) content (Fig. 1g,h). Further, evaluation of fibrotic protein markers in total lung homogenates showed markedly lower expression of both α-smooth muscle actin (αSMA, a marker of myofibroblast differentiation) and type I collagen in bleomycin-challenged *ephrinb2*-CKO mice compared to controls (Fig. 1i).

Identification of soluble ephrin-B2 ectodomain in bronchoalveolar lavage fluid

Given the requirement for ephrin-B2 fibroblast expression that we identified in bleomycin-induced lung fibrosis, we next investigated the regulation of ephrin-B2 expression in this model. Lung homogenates from wild type (WT) mice 14 d post-bleomycin did not demonstrate greater expression of the full-length transmembrane ephrin-B2 (approximately 60 KDa, as previously described for fibroblasts, endothelial cells and cancer cells[18]) compared to homogenates from WT mice post-PBS challenge, but rather the appearance of a lower molecular weight band (~50 kDa) that was either absent or expressed at low levels in lungs post-PBS challenge (Fig. 2a).

Ephrin-B ligands, as well as EphB receptors, have been shown to undergo ectodomain shedding to release active proteins[19-22]. Proteolytic cleavage of mouse ephrin-B2 has recently been shown to generate a 50 kDa band corresponding to ephrin-B2's ectodomain, consistent with our findings in Fig. 2a[23]. These data led us to hypothesize thatephrin-B2 is proteolytically cleaved following pro-fibrotic lung injury, and that the resulting soluble form of ephrin-B2's ectodomain (sEphrin-B2) contributes to the pathogenesis of fibrosis. To investigate this hypothesis, we first evaluated the presence of sEphrin-B2 in bronchoalveolar lavage (BAL) post-bleomycin challenge. As demonstrated by Western blotting with an N-terminus-specific anti-ephrin-B2 antibody, sEphrin-B2 expression was observed at low basal levels in BAL from 14 d post-PBS treated WT mice, but was markedly greater in BAL from WT mice 14 d post-bleomycin (Fig. 2b,c). Further, using an ELISA with an ectodomain-specific anti-ephrin-B2 detection mAb, we observed greater sEphrin-B2 concentrationin BAL from bleomycin-challenged mice at 3, 7 and 14 days post-bleomycin challenge compared to PBS-challenged mice (Fig. 2d).

Oligomeric sEphrin-B2 directs fibroblast migration, invasion and myofibroblast differentiation

To investigate whether generation of sEphrin-B2 was reduced in *ephrinb2*-CKO mice following bleomycin challenge, which could contribute to the protection of these mice from lung fibrosis in this model, we compared concentration of sEphrin-B2 in BAL of *ephrinb2*-CKO and *ephrinb2*-C in mice 14 d post-bleomycin treatment. sEphrin-B2 concentration was lower, but not completely eliminated, in BAL from *ephrinb2*-CKO mice compared to *ephrinb2*-C mice 14 d post-bleomycin treatment (Fig. 2e). We hypothesized that this reduction was at least in part attributable to loss of sEphrin-B2 generation from ephrin-B2-deficient fibroblasts; i.e. that fibroblasts in WT mice are a source of sEphrin-B2 generated in response to lung injury. To test this hypothesis, we assessed sEphrin-B2 shedding by lung

fibroblasts isolated from PBS- or bleomycin-challenged WT mice by ELISA. Low concentration of sEphrin-B2 was present in media conditioned by lung fibroblasts isolated from PBS-challenged WT mice. In contrast, media conditioned by lung fibroblasts isolated from WT mice 7 d post-bleomycin challenge had markedly higher concentration of sEphrin-B2 (Fig. 2f). Furthermore, concentration of sEphrin-B2 was substantially lower in media conditioned by lung fibroblasts isolated from PBS- or bleomycin-challenged fibroblasts that had been transfected with siRNA targeting ephrin-B2, compared to media conditioned by these fibroblasts transfected with non-targeting control siRNA (Fig. 2f).

We next determined whether the ephrin-B2 ectodomain that is shed as sEphrin-B2 from fibroblasts and present in BAL following lung injury directs pro-fibrotic fibroblast activities. In these experiments, we used mouse recombinant-ephrin-B2-Fc, which contains ephrin-B2's ectodomain, fused to an Fc-domain that replaces the transmembrane and C-terminal domains of full-length ephrin-B2 protein (Fig. 3a). Structural and functional studies have demonstrated that EphB receptor activation requires higher order ephrin-B2 oligomers[24]; we consequently pre-clustered ephrin-B2-Fc for these experiments by incubating mouse ephrin-B2-Fc with IgG antibody at a 2:1 ratio immediately before use. Treatment of mouse lung fibroblasts with pre-clustered ephrin-B2-Fc, but not pre-clustered ephrin-B1-Fc or ephrin-B3-Fc, markedly increased filopodia formation (Fig. 3b,c), suggesting that ephrin-B2, but not -B1 or -B3, can regulate fibroblast motility. Chemotaxis assays demonstrated that pre-clustered ephrin-B2-Fc induced fibroblast migration in a dose-dependent manner similar to chemotactic agents such as lysophosphatidic acid (LPA) or platelet-derived growth factor (PDGF-BB) (Fig. 3d). These findings indicate sEphrin-B2 contributes to fibroblast chemotaxis.

The ephrin-B2 ligand signals through the EphB subfamily of receptor tyrosine kinases, which includes EphB1-4 and Eph6 (EphB5 is present in chickens, but no mammalian homologue has been identified)[25]. Primary mouse lung fibroblasts expressed EphB2, EphB3 and EphB4 receptors but not EphB1 or EphB6 (Fig. 3e). Individual siRNA knockdown of these receptors revealed that both fibroblast chemotaxis and fibroblast invasion through matrigel induced by BAL from bleomycin-treated mice required both EphB3 and EphB4, but not EphB2 receptor signaling (Fig. 3f,g).

As EphB receptor activation requires higher order ephrin-B2 oligomers as noted above[24], we investigated the quaternary structure of sEphrin-B2 in BAL by immunoblotting BAL proteins that had been separated by native-PAGE on non-reducing gels. Our N-terminus-specific anti-ephrin-B2 mAb recognized high molecular weight species consistent with higher order sEphrin-B2 oligomers in BAL from bleomycin-challenged but not control mice (Fig. 3h). These higher order species were not recognized in BAL samples pre-treated with SDS and 2-mercaptoethanol, further indicating that sEphrin-B2 is present in the form of higher order oligomers in BAL recovered from mice following lung injury. Competition studies performed by pre-incubating our N-terminus-specific anti-ephrin-B2 mAb with recombinant ephrin-B2 prior to immunoblotting were consistent with this antibody binding to sEphrin-B2 in the oligomers (Supplementary Fig. 1). Our results suggest that sEphrin-B2 oligomers are present in BAL following lung injury and are biologically active in terms of being able to mediate pro-fibrotic functions of fibroblasts. Consistent with this hypothesis,

depletion of sEphrin-B2 in BAL from bleomycin-challenged mice with magnetic beads coated with the N-terminus-specific anti-ephrin-B2 mAb markedly though not completely reduced the fibroblast chemotaxis that was induced by these BAL samples (Fig. 3j).

We next determined whether ephrin-B2 signaling could also induce fibroblast-to-myofibroblast differentiation. Treatment of primary mouse lung fibroblasts with pre-clustered ephrin-B2-Fc markedly increased mRNA and protein expression of α-SMA and collagen type I compared to IgG-Fc treatment (Fig. 3k,l).

Ephrin-B2 ectodomain is sufficient to drive tissue fibrosis *in vivo*

Asephrin-B2 ectodomain can direct pro-fibrotic fibroblast functions *in vitro,* we next investigated whether recombinant Ephrin-B2-Fc can induce tissue fibrosis *in vivo.* Mice were injected subcutaneously with pre-clustered mouse ephrin-B2-Fc (100μg/kg/mouse), or IgG-Fc as a control, daily for two weeks. Blinded histological analysis showed that Ephrin-B2-Fc treatment produced robust dermal fibrosis (Fig. 3m) associated with markedly increased dermal thickness (Fig. 3n), hydroxyproline content (Fig. 3o), and α-SMA and type I collagen expression (Fig. 3p) compared to IgG-Fc treatment. While these data demonstrate that ephrin-B2 forward signaling by ephrin-B2's ectodomain is sufficient to drive myofibroblast formation and tissue fibrosis *in vivo*, we have not investigated potential contributions of ephrin-B2's ectodomain on other cell types, such as endothelial or immune cells.

In addition to lung fibrosis, we assessed the role of ephrin-B2 in the development of skin fibrosis *in vivo.* We subjected *ephrinb2-*CKO mice and *ephrinb2-*C mice to the bleomycin model of dermal fibrosis (Fig. 3q). Blinded histological analysis showed markedly attenuated skin fibrosis in bleomycin-treated *ephrinb2-*CKO mice, associated with considerably lower dermal thickness and hydroxyproline content compared to control animals (Fig. 3r,s).

Identification of ADAM10 as the ephrin-B2 ectodomain sheddase in fibroblasts

Previous studies have shown that ephrins can be cleaved by metalloproteinases, including matrix metalloproteinases (MMPs) and disintegrin and metalloproteases (ADAMs)[19-22]. In order to investigate whether ephrin-B2 ectodomain shedding is regulated by metalloproteinases in fibroblasts, we tested the ability of BB-94, a broad-spectrum inhibitor of both MMPs and ADAMs, to inhibit fibroblast generation of sEphrin-B2. BB-94 treatment dose-dependently reduced sEphrin-B2 concentration in media conditioned by normal human lung fibroblasts, indicating that metalloproteinase(s) contribute to ephrin-B2 cleavage (Fig. 4a). Of the MMPs and ADAMs, these fibroblasts expressed MMP-1, MMP2 and MMP14 as well as ADAM9, ADAM10, ADAM12 and ADAM17 (Fig. 4b). In order to investigate whether any of these proteases act as ephrin-B2 ectodomain sheddases in human lung fibroblasts, we performed siRNA knockdowns of each of these metalloproteinases individually. We first confirmed that siRNA duplexes efficiently knocked down the MMPs and ADAMS we found to be expressed by cultured primary human lung fibroblasts (Supplementary Fig. 2). We then found that siRNA-mediated knockdown of *ADAM10*, but

not the other ADAMs or MMPs expressed by fibroblasts, markedly lowered sEphrin-B2 concentration in fibroblast cell culture supernatant, as assessed by ELISA (Fig. 4c).

To further investigate whether ADAM10 is responsible for ephrin-B2 ectodomain shedding in fibroblasts, we used phorbol 12-myristate 13-acetate (PMA), which activates limited proteolysis of membrane-bound proteins, *i.e.* ectodomain shedding, by increasing the activity of ADAM10 and ADAM17[26]. Treatment of human lung fibroblasts with PMA for 30 min resulted in marked increase in sEphrin-B2 concentration in fibroblast cell culture supernatants (Fig. 4c). Knockdown of *ADAM10* by siRNA also substantially reduced sEphrin-B2 concentration in media-conditioned by PMA-stimulated fibroblasts, whereas knockdowns of *ADAM17* or other ADAMs or MMPs had no pronounced effects. Moreover, treatment of fibroblasts with GX254023X, an ADAM10-specific inhibitor, reduced both constitutive and PMA-stimulated sEphrin-B2 concentration in fibroblast supernatants in a dose-dependent manner (Fig. 4d). In contrast, fibroblast treatment with TAPI-0, an ADAM17-specific inhibitor, did not prevent sEphrin-B2 generation by fibroblasts (Fig. 4d), further implicatingADAM10 in ephrin-B2 shedding.

ADAM10-mediated ephrin-B2 shedding drives TGF-β-induced myofibroblast activation

Having identified ADAM10 as the major ephrin-B2 ectodomain sheddase in fibroblasts, we then investigated the regulation of this shedding, and its contribution to the pro-fibrotic activities of these cells. Transforming growth factor-β1 (TGF-β1) is a prototypical pro-fibrotic cytokine that induces myofibroblast activation[27,28]. Whereas TGF-β1 treatment of human lung fibroblasts did not induce expression of *ephrin-B2* mRNA, it did result in greater *ADAM10* mRNA expression in these cells compared to untreated cells (Fig. 4e), and substantially greater sEphrin-B2 concentration in media conditioned by these cells compared to untreated cells (Fig. 4f).

Given that we found that recombinant ephrin-B2-Fc induces fibroblast differentiation into activated myofibroblasts *in vitro*, and resulted in greater expression of the myofibroblast marker α-SMA in mice *in vivo*, we investigated whether TGF-β-induced myofibroblast activation is dependent on ephrin-B2 shedding. Genetic knockdown of *ADAM10*, or pharmacological inhibition with the ADAM10-selective inhibitor GX254023X[29], reduced TGF-β-induced sEphrin-B2 production, confirming the role of ADAM10 in TGF-β-induced ephrin-B2 shedding (Fig. 4f,g). TGF-β-induced α-SMA protein expression by human lung fibroblasts was also markedly reduced by siRNA knockdown of *ADAM10* (Fig. 4h), or by pharmacological inhibition of ADAM10 with GX254023X, which reduced TGF-β-induced *ACTA2* mRNA expression dose-dependently (Fig 4i). GX254023X treatment also markedly and dose-dependently reduced TGF-β-induced α-SMA protein expression by human lung fibroblasts (Fig 4j). Further, immunofluorescence staining of human lung fibroblasts with an anti-α-SMA antibody and rhodamine-phalloidin demonstrated that GX254023X treatment inhibited TGF-β-induced stress fiber formation and incorporation of α-SMA protein into stress fibers, both phenotypic characteristics of activated myofibroblasts (Fig. 4k). Taken together, these results indicate that TGF-β-induced myofibroblast formation requires ADAM10-mediated ephrin-B2 shedding.

Previous studies have shown that ADAM10 cleaves ephrin-B2 in the juxtamembrane region of its ectodomain[20,30] (Fig. 4l). We therefore tested whether this region is important for TGF-β-induced ephrin-B2 shedding and myofibroblast activation. Forced overexpression of ephrin-B2 [Ecto], which lacks the entire ephrin-B2 ectodomain but preserves the transmembrane and intracellular domains, markedly reduced the amount of sEphrin-B2 produced by these cells in response to TGF-β, compared to the amount of sEphrin-B2 produced by TGF-β challenge of fibroblasts transfected with wild type (WT) ephrin-B2 (Fig. 4l,m). Likewise, overexpression of a juxtamembrane deletion mutant, ephrin-B2 [Juxta], which lacks amino acids 168-218 of the ephrin-B2 ectodomain, abrogated TGF-β-induced ephrin-B2 shedding (Fig. 4l,m). Further, deletions of specific sequences in the juxtamembrane region (amino acids 182–194 or 197–218) rendered ephrin-B2 resistant to TGF-β-induced ephrin-B2 shedding (Fig. 4l,m).

To further demonstrate that ephrin-B2's juxtamembrane region is required for ephrin-B2 shedding induced by TGF-β, we analysed ephrin-B2 protein levels in fibroblasts transfected with HA-tagged WT ephrin-B2 or HA-tagged, cleavage-resistant mutants. As shown in Fig. 4n, the amount of HA-tagged WT ephrin-B2 that was detected by anti-HA antibodies in lysates of human lung fibroblasts was substantially reduced by TGF-β treatment, consistent with TGF-β inducedephrin-B2 shedding. In contrast, this TGF-β-induced reduction in HA-tagged ephrin-B2 expression was largely prevented in human lung fibroblasts overexpressing HA-tagged, cleavage-resistantephrin-B2 mutants, further demonstrating the requirement of ephrin-B2'sjuxtamembrane region forectodomain cleavage (Fig. 4n).

We next investigated whether overexpression of cleavage-resistant ephrin-B2 mutants prevents TGF-β-mediated myofibroblast activation, in addition to ephrin-B2 shedding. We found that human lung fibroblasts overexpressing cleavage-resistant ephrin-B2 mutants had reduced TGF-β-induced *α-SMA* mRNA and protein levels compared to human lung fibroblasts transfected with WT ephrin-B2 (Fig. 4o,p), consistent with ephrin-B2 cleavage being required for TGF-β-induced myofibroblast activation.

As recombinant ephrin-B2 ectodomain was sufficient to drive myofibroblast activation, and TGF-β-induced myofibroblast activation required ADAM10-mediated ephrin-B2 shedding, we hypothesized that TGF-β-induced myofibroblast activation is controlled by autocrines Ephrin-B2/EphB receptor signalling. Of the five identified EphB receptors, primary human lung fibroblasts expressed *EphB3* and *EphB4* but not *EphB1, EphB2,* or *EphB6* (Fig. 4q). We found that siRNA-mediated knockdown of *EphB3* or *EphB4* markedly reduced TGF-β-induced increase in both *ACTA2* mRNA and α-SMA protein levels compared to human lung fibroblasts transfected with non-targeting siRNA (Fig. 4r,s), demonstrating that both receptors mediate pro-fibrotic activities of sEphrin-B2 in lung fibroblasts.

Pharmacological inhibition of ADAM10 prevents bleomycin-induced lung fibrosis in mice

Based on our findings above, we hypothesized that therapeutic targeting of ADAM10, with the ADAM10-selective pharmacological inhibitor GX254023X[29], could prevent lung fibrosis by inhibiting ephrin-B2 shedding and myofibroblast activation *in vivo*. Previous studies show that bleomycin challenge rapidly increases levels of activated TGF-β within areas of lung injury[31,32], which led us to hypothesize that ADAM10 levels would be

similarly increased upon lung injury. Indeed, ADAM10 expression levels were markedly higher *in vivo* after bleomycin-induced lung injury compared to PBS-challenged mice (Fig. 5a). To examine the ability of ADAM10 inhibition to mitigate lung fibrosis *in vivo*, mice were subjected to the bleomycin-induced lung fibrosis model and treated daily with GI254023X (200 mg/kg/day) or vehicle control by intraperitoneal injection. Blinded histological analysis revealed that lung parenchymal fibrosis produced 14 days post-bleomycin challenge in vehicle-treated mice was mitigated in mice treated with GX254023X (Fig. 5b), associated with marked reduction in lung hydroxyproline levels (Fig. 5c). ADAM10 inhibition also resulted in a considerable lower level of α-SMA expression in bleomycin-challenged mice compared to PBS-challenged mice (Fig. 5d).

To gain insight into GX254023X's mechanism of action in this lung fibrosis model, we assessed sEphrin-B2 concentration in BAL samples. Consistent with our *in vitro* studies demonstrating that ADAM10 is responsible for ephrin-B2 cleavage to generate sEphrin-B2, GX254023X treatment reduced sEphrin-B2 concentration in the BAL of bleomycin-challenged mice (Fig. 5e), suggesting that the ADAM10/sEphrin-B2 axis drives myofibroblast activation in lung fibrosis *in vivo*. Further, ADAM10 inhibition with GX254023X markedly reduced mortality caused by bleomycin-induced lung injury and fibrosis in mice (Fig. 5f).

The ADAM10-mediated ephrin-B2 shedding pathway is upregulated in idiopathic pulmonary fibrosis

To determine the relevance of our studies to human disease, we investigated the role of ADAM10/sEphrin-B2 signaling on fibroblasts isolated from the lungs of individuals with IPF and normal controls. IPF lung fibroblasts had substantially higher concentration of sEphrin-B2 in culture media and expressed markedly increased *ADAM10* mRNA compared to normal lung fibroblasts *in vitro* (Fig. 6a,b). Pharmacological inhibition of ADAM10 with GX254023X, or siRNA knockdown of *ADAM10*, both markedly reduced sEphrin-B2 production by both IPF and control lung fibroblasts (Fig. 6c,d), confirming that ADAM10 is responsible for ephrin-B2 shedding in IPF and control lung fibroblasts. IPF lung fibroblasts are characterized by increased collagen type I and α-SMA expression[33]. We examined whether ADAM10/sEphrin-B2 signaling contributes to this increased expression of *collagen 1a1* and *ACTA2* by inhibiting ADAM10 in IPF lung fibroblasts. Treatment with GX254023X or siRNA targeting ADAM10 markedly inhibited the increased *collagen 1a1* and *ACTA2* expression of IPF fibroblasts compared to controls (Fig. 6e,f,g,h).

Given the relevance of the ADAM10/sEphrin-B2 axis in IPF lung fibroblasts, we next examined concentration of sEphrin-B2 in both BAL fluid and plasma samples from individuals with IPF and healthy volunteers. Quantification of sEphrin-B2 in these samples by ELISA, and by western blotting of a subset of these samples, showed markedly increased concentration of sEphrin-B2 in the BAL fluid of 16 individuals with IPF compared to samples from eight healthy volunteers (Fig. 6i,j). We then compared plasma sEphrin-B2 concentration in 30 individuals with IPF and 30 gender-matched, non-smoking controls (subject demographics in Supplementary Table 1), and observed a markedly higher

concentration of plasma sEphrin-B2 in the IPF individuals compared to the samples from the control group (Fig. 6k).

Discussion

Using a combination of mouse models and clinical samples obtained from individuals with IPF, we demonstrate that a soluble form of ephrin-B2, composed of its cleaved ectodomain, is a potent mediator of tissue fibrosis. This soluble form, sEphrin-B2, was markedly elevated in the lung tissue and BAL of mice in our pulmonary fibrosis model, and in the BAL of individuals with IPF, suggesting ephrin-B2 shedding is increased in response to tissue injury. We demonstrate that recombinant Ephrin-B2 ectodomain was sufficient to induce dermal fibrosis in mice when injected subcutaneously by promoting collagen and α-SMA expression consistent with myofibroblast activation. Conversely, loss of ephrin-B2 in fibroblasts of mice resulted in decreased sEphrin-B2 generation and protection from lung and dermal fibrosis *in vivo*, identifying ephrin-B2 as a critically important pro-fibrotic mediator. Although loss of ephrin-B2 in fibroblasts provided substantial protection from bleomycin-induced skin and lung fibrosis, we did not observe full protection in both models, suggesting additional cell types such us inflammatory cells may also be sources of soluble ephrin-B2 during the development of tissue fibrosis, which will be the focus of future investigations.

Both ephrin-B ligands and EphB receptors have previously been demonstrated to undergo ectodomain shedding to release active proteins[19-22]. In cancer cells, shedding of membrane-bound ephrin B ligands regulates invasion[34]. To the best of our knowledge, however, our study is the first to describe ephrin-B2 shedding in tissue fibrosis, and to implicate sEphrin-B2 in human fibrotic disease. Our results suggest a new regulatory mechanism during tissue fibrogenesis, in which proteolytic shedding of the ectodomain of ephrin-B2 amplifies myofibroblast activation and pro-fibrotic functions. Our studies demonstrate that the generation of sEphrin-B2 by fibroblasts inducedephrin-B2 forward signaling through EphB3 and EphB4, is involved in multiple fibroblast functions, including migration, invasion, myofibroblast differentiation and collagen production.

Our study also identified ADAM10 as the major metalloprotease responsible for the generation of sEphrin-B2 by human lung fibroblasts. Ephrin-B2 cleavage by ADAM10 has recently been demonstrated during Xenopus development[20], suggesting an evolutionarily conserved mechanism for ephrin-B2 cleavage by ADAM10 in both development and tissue fibrogenesis. The aberrant reactivation of multiple developmental pathways has been implicated in the pathogenesis and progression of lung fibrosis[35,36], and our results suggest that ADAM10/ephrin-B2 may be another such pathway. Consistently, our results suggest that the ADAM10-mediated ephrin-B2 shedding pathway is reactivated by tissue injury, and its sustained activation promotes organ fibrosis by sustaining and amplifying myofibroblast activation.

We also identified EphB3 and EphB4 as the receptors through which the ADAM10/sEphrin-B2 pathway directs myofibroblast activation. Importantly, our results demonstrate that sEphrin-B2 produced in the alveolar space upon lung injury is the form of active high

molecular weight oligomers. Activation of forward EphB receptor signalling requires Eph receptor clustering induced by binding of oligomeric ephrins. Our results demonstrate that this oligomeric state of sEphrin-B2 in fibrotic tissues is biologically active and regulates myofibroblast functions. Consequently, strategies to interrupt the elaboration of sEphrin-B2 by fibroblasts, by targeting ADAM10, have the potential to serve as novel therapeutic strategies for fibrotic diseases. As we found, therapeutic targeting of ADAM10 with GX254023X was able to substantially reduce lung fibrosis in mice by inhibiting ephrin-B2 shedding and myofibroblast activation *in vivo*, providing preclinical evidence that inhibition of ADAM10 could mitigate fibrosis *in vivo*.

During our investigations into the molecular mechanism(s) through which ADAM10-mediated ephrin-B2 shedding is activated in fibroblasts, we determined that this pathway was activated by TGF-β, the prototypical cytokine that drives myofibroblast activation. We found that fibroblast ADAM10 expression, but not expression of ephrin-B2 itself, is induced by TGF-β signaling. Further, we found that genetic or pharmacological inhibition of ADAM10-mediated ephrin-B2 shedding blocked myofibroblast activation by TGF-β, indicating that ephrin-B2 cleavage is required for the generation of myofibroblasts, central effector cells in the development of fibrosis. Currently, how ADAM10 mediates ephrin-B2 cleavage in fibroblasts is not fully understood. Previous studies have shown that ADAM10 cleaves the juxtamembrane regions of ephrin-A2[22] and ephrin-B2[20] to release active ectodomains. Consistent with these data, our genetic studies overexpressing cleavage-resistant ephrin-B2 mutants confirmed the requirement for ephrin-B2's juxtamembrane region in ADAM10-mediated ephrin-B2 shedding and myofibroblast activation by TGF-β. The molecular requirement for ADAM10-mediated ephrin-B2 shedding in myofibroblast activation by TGF-β warrants further investigation. Previous studies have shown that ephrin-B2 and EphB4 receptor interact on the surface of the same cell (*i.e.*, in "cis"), and this interaction attenuates the ability of ephrin-B2 expressed in other cells to activate forward ephrin-B2:EphB4 receptor signalling in "trans"[37]. Our studies on human lung fibroblasts may suggest a molecular mechanism in which high expression of membrane-bound ephrin-B2 in quiescent fibroblasts prevents activation of forward EphB3/B4 receptor signalling via "cis" negative interaction. Upon tissue injury, TGF-β-mediated ADAM10 upregulation would lead to increased ephrin-B2 shedding in activated myofibroblasts. Consequently, ADAM10-mediated ephrin-B2 shedding could promote:(a) de-repression of the negative "cis" inhibitory ephrin-B2:EphB3/B4 receptor interaction, and/or (b) activation of pro-fibrotic forward EphB3/B4 receptor signalling activated by autocrine sEphrin-B2, although ephrin-B2 expressed in other cells implicated in pathological fibrosis could be involved in activation of EphB3/B4 receptors "in trans". Further research focused on gathering mechanistic understanding of ephrin-B2 signalling in activated myofibroblasts is needed.

Although our study does not address whether ephrin-B2 reverse signaling may also regulate myofibroblast activation or function, ephrin-B2 ectodomain shedding would concomitantly terminate ephrin-B2 reverse signaling through ephrin-B2's cytoplasmic tail infibroblasts previously bearing full-length ephrin-B2. Reverse ephrin-B2 ligand signaling has recently been shown to play an anti-fibrotic role in mouse models of kidney fibrosis by protecting against peritubular capillary rarefaction by promoting angiogenesis and vascular stability during kidney injury, and, most relevant to our study, inhibiting pericyte-to-myofibroblast

transition and myofibroblast activation[14]. Thus ephrin-B2 ectodomain shedding may not only promote myofibroblast activation by promoting pro-fibrotic ephrin-B2 forward signaling, but also by terminating anti-fibrotic ephrin-B2 reverse signaling.

Our studies also show that ADAM10/sEphrin-B2 signaling is upregulated in fibroblasts from individuals with idiopathic pulmonary fibrosis and elevated concentration of sEphrin-B2 in plasma and BAL from individuals with IPF. These data further emphasize on the relevance of ADAM10/sEphrin-B2 signaling in human disease.

In summary, we have identified a novel pathway that promotes myofibroblast activation and effector functions through ADAM10 cleavage of ephrin-B2 to generate sEphin-B2 that signals through EphB3 and EphB4. This pathway is required for TGF-β-induced myofibroblast activation, suggesting it plays a central role in the pathogenesis of fibrotic diseases. Our study also identifies sEphrin-B2, its receptors EphB3/EphB4, and its sheddase ADAM10 as potential therapeutic targets for this class of diseases (Fig. 6l).

Materials and Methods

Plasmids, antibodies and reagents

Ephrin-B2 plasmids including HA-tagged full-length *ephrin-B2^{wildtype}*, *ephrin-B2 $^{Ecto-HA}$*, *ephrin-B2 $^{Juxta-HA}$*, *ephrin-B2 $^{182-194-HA}$* and *ephrin-B2 $^{197-218-HA}$* were kindly shared by Ira O. Daar (National Cancer Institute, National Institutes of Health, USA). Mouse and human recombinant PDGF-BB, ephrin-A1, ephrin-A2, ephrin-A3, ephrin-A4, ephrin-A5, ephrin-B1, ephrin-B2 and ephrin-B3 were purchased from R&D Systems, 18:1 LPA from Avanti Polar Lipids. Antibodies used for Western blotting include: mouse polyclonal anti-α-SMA (clone 1A4; Sigma-Aldrich), rabbit polycloncal collagen type I (ab34710, Abcam), rabbit monoclonal GAPDH (clone D16H11, Cell Signaling), mouse monoclonal β-actin (AC-15, Sigma), ephrin-B2 (P-20 Santa Cruz and HPA008999 Sigma), ADAM10 (#14194, Cell Signaling) and rabbit monoclonal HA-Tag (C29F4, Cell Signaling). Pharmacological inhibitors including BB-94 (Batimastat), GI254023X and TAPI-0 as well as phorbol 12-myristate 13-acetate (PMA), 4-hydroxytamoxifen, and fibronectin were purchased from Sigma-Aldrich. Recombinant human and mouse TGF-beta 1 protein was purchased from R&D.

Cell lines

Human lung fibroblasts (IMR-90) were purchased from ATCC and cultured according to the vendor's protocol. Cell cultures were tested for mycoplasma infection.

Animals

Pathogen-free female C57BL/6N (6-8-week-old) mice purchased from the National Cancer Institute (NCI)-Frederick Mouse Repository (Frederick, MD, USA) were used throughout this study. All experiments were performed in accordance with National Institute of Health guidelines and protocols approved by the Massachusetts General Hospital Subcommittee on Research Animal Care, and maintained all mice in a specific pathogen–free (SPF)

environment certified by the American Association for Accreditation of Laboratory Animal Care (AAALAC).

Generation of ephrin-B2 conditional-knockout mice

To generate mice in which ephrin-B2 could be conditionally deleted specifically in collagen-expressing cells such as fibroblasts (*ephrin-B2 conditional knockout*, *ephrinb2*-CKO mice), C57BL/6N mice carrying a tamoxifen-inducible Cre-recombinase [*Col1a2-Cre/ERT*] (Jackson laboratory) were crossed with *Efnb2^loxP/loxP* mice[17]. Mice homozygous for the *ephrin-B2F* allele and hemizygous for the *Col1a2-Cre/ERT* allele [*Efnb2^loxP/loxP*; *Col1a2-Cre/ERT*] were generated. Genotyping was performed using specific primers for *Cre* and *ephrin-B2* (Supplementary Table 2). 3-week old *Efnb2^loxP/loxP*; *Col1a2-Cre/ERT* mice were treated with intraperitoneal injections of the tamoxifen suspension (0.1 ml of 10 mg/ml) to delete *ephrin-b2* or corn oil (as control) for 7 days. Successful loss of ephrin-B2 expression upon tamoxifen treatment in lung fibroblasts was confirmed by western blotting using anti-ephrin-B2 antibody. All animal procedures and protocols were approved by the Comité Institutionnel de protection des animaux (Institutional Animal Protection Committee) of the University of Montreal Hospital Research Centre (CRCHUM), animal care committee of the Krembil Research Institute (University Health Network) and Massachusetts General Hospital Subcommittee on Research Animal Care.

Mouse model of pulmonary fibrosis

Six-weeks old mice were anesthetized with ketamine and xylazine before exposure of the trachea. Lung fibrosis was induced by intratracheal administration of bleomycin (50 μl at 1.2 U/kg) or phosphate buffered saline (PBS; as control) as previously described[38,39]. Mice were sacrificed at indicated time points. Lungs and BAL were harvested for histological studies, collagen determination and biochemical analyses.

For *in vivo* drug studies with ADAM10 inhibitor, GI254023X was diluted in 0.1 M carbonate buffer and mice were administered 200 mg/kg once daily by intraperitoneal injection with a total volume of 100 μl. Drug dosing began 3 days prior to bleomycin or PBS treatment and was maintained daily throughout the course of the study.

Mouse model of skin fibrosis

Skin fibrosis in 6-8 week-old mice was induced by daily subcutaneous injection of bleomycin (100 μl from 10 μg/ml stock) for 28 days as previously described[27]. Sterile saline was used as control. Mice were then sacrificed, and full-thickness 6 mm punch biopsies were obtained to conduct histological, immunohistochemical and hydroxyproline analysis.

Generation of Ephrin-B2 immune complexes

To generate ephrin-B2 immune complexes, recombinant mouse or human ephrin-B2-Fc (R&D systems) was incubated at a 2:1 ratio (wt/wt) with a goat antibody against human IgG (Jackson ImmunoResearch) for 90 min at 4 °C before immediate use.

In vivo ephrin-B2-Fc injection

Subcutaneous injections using mouse recombinant ephrin-B2-Fc were performed using the methodology previously reported for bleomycin-induced model of skin fibrosis[40]. 6-8 week old mice received 100μl subcutaneous injections of pre-clustered ephrin-B2-Fc (100μg/Kg/ mouse) into a single location on the shaved back of mice once daily for 2 weeks. Control mice received subcutaneous injections of IgG Fc for 2 weeks. Following two-week treatment with either IgG-Fc or ephrin-B2-Fc, mice were further housed for 2 weeks and sacrificed by CO_2 euthanasia and skin samples were collected for histological studies, collagen determination and biochemical analyses. All animal procedures and protocols were approved by the Comité Institutionnel de protection des animaux (Institutional Animal Protection Committee) of the University of Montreal Hospital Research Centre (CRCHUM), animal care committee of the Krembil Research Institute (University Health Network) and Massachusetts General Hospital Subcommittee on Research Animal Care.

Histological analysis

Excised skin and lung biopsies were fixed in 10% buffered formalin and multiple paraffin-embedded 5-μm sections of the entire mouse lung and skin were stained with hematoxylin and eosin (H&E) or Masson's Trichrome according to the standard protocols of our laboratory as previously described[27,39].

Dermal thickness measurement

Dermal thickness was determined with the use of photomicrographs (100× magnification) of H&E-stained sections, measuring the distance between the epidermal–dermal junction and the dermal–fat junction at 5 randomly selected sites per high power field in 10 high-power fields per section as previously shown[27]. All investigations were performed in a blinded fashion.

Hydroxyproline assay

Collagen content in mouse lungs and skin were measured using hydroxyproline assay as previously described[27,38,39].

Mouse BAL recovery

To obtain BAL samples for chemoattractant activity analysis, ephrin-B2 ELISA and total protein concentration determination, lungs were lavaged with six 0.5-ml aliquots of PBS. BAL samples were centrifuged at 3,000g for 20 min at 4°C and transferred the supernatants to siliconized low-binding Eppendorf tubes (PGC Scientifics) for subsequent analysis.

BAL total protein

Total protein concentration in BAL samples was determined using a commercially available bicinchoninic acid BCA Protein Assay Kit (Pierce) as per manufacturer's protocol.

Determination of Ephrin-B2 levels in BAL and plasma

Soluble ephrin-B2 levels in human and mouse BAL fluids and human plasma were determined by ELISA (Uscn Life Science Inc., SEE112Hu, SEE112Mu) according to the manufacturer's protocol.

Preparation of ephrin-B2 antibody-coated beads

Ephrin–B2 antibody (1-2 μg) was chemically cross-linked to 2.8 μm superparamagnetic Dynabeads® M-270 Epoxy beads (Life Technologies) according to the manufacturer's protocol. Beads were washed with PBS and then blocked for 1 h in 2% (w/v) BSA (bovine serum albumin)/PBS before re-suspension in PBS. Ephrin-B2 was immunoprecipitated by incubation of BAL fluids with ephrin-B2 antibody-coated beads overnight at 4°C. Ephrin-B2-depleted BALs were used as chemoattractants in migration and invasion assays.

Isolation of primary mouse lung fibroblasts

Primary lung fibroblasts were isolated as previously described[38].

Fibroblast chemotaxis and invasion assay

Fibroblast chemotaxis was assayed using a 96-Multiwell FluoroBlok™ Inserting system (Fisher Scientific, pore size: 8 μm) pre-coated with fibronectin at 10 μg/mL (Sigma). Briefly, cells were labeled with DiIC12(3) Fluorescent Dye for 1 hour prior to chemotaxis. 50,000 cells in 50 μL serum-free DMEM were then added to the apical chambers and exposed to BAL or BAL fractions, ephrin-B2-Fc, 18:1 LPA (Avanti Polar Lipids) or PDGF-BB (R&D Systems) as chemoattractants. The plate was then incubated for 4 hours at 37°C, 5% CO2 atmosphere. Fluorescence of migrated cells was recorded at 544/590 nm (Ex/Em) on a bottom-reading fluorescent plate reader using Fluoroskan Ascent FL (Thermo). The data were expressed as the ratio of migrated cells towards any chemoattractant to cells migrated towards serum-FREE DMEM. Experiments were performed in triplicates. For invasion assays, a 96-well BioCoat Tumor Invasion System (Fisher Scientific) was used and plate was read at 48 hours. Cells at passages 3 to 5 were used for chemotaxis and invasion assays. To test the effect of receptor inhibition, fibroblasts were transfected with siRNA to *EPHB2*, *EPHB3* or *EPHB4* receptor before addition of BAL as chemoattractant.

siRNA and plasmid transfection

The siRNA duplexes targeting human ephrin-B2, human *MMP1*, human *MMP2*, human *MMP7*, human *MMP14*, human *ADAM9*, human *ADAM10*, human *ADAM12*, human *ADAM17*, human *EPHB3*, human *EPHB4*, mouse ephrin-B2, mouse *EphB2*, mouse *EphB3* and mouse *EphB4* mRNA were On-Target Plus Smart Pools and were obtained from Dharmacon Inc. (Thermo Scientific). The siRNAs (20 nM) were transiently transfected into human and mouse primary fibroblasts using HiPerFect Reagent (Qiagen) at ansiRNA/HiPerFect ratio of 1:4 (μg/μl). On-Target Plus non-targeting siRNA pool were used as a nonspecific control. Cells were harvested and mRNA levels were assessed 48 hours after transfection. Transient transfection experiments with ephrin-B2 mutants were performed on primary human and murine lung fibroblasts seeded on 6-well plates (60-70% confluency) using lipofectamine 2000 (Thermo Fisher Scientific).

Filopodia formation

Filopodial protrusions at the cell front were analysed from 20 microscopic fields on 25-50 cells per conditions..

RT-PCR and qRT-PCR

Total RNA was extracted using Qiagen extraction kits according to the manufacturer's protocol, and cDNAs were generated by reverse transcription using iScript™ cDNA Synthesis Kit (BioRad) as previously reported[39]. Quantitative PCR was performed using fluorogenic SYBR Green and Mx4000 Multiplex Quantitative PCR System (Stratagene) as previously described[39]. *GAPDH* was used as reference gene in all qRT-PCR reactions. PCR was performed using the primers listed in Supplementary Table 2 at a final concentration of 100 nM. Relative transcript abundance of a gene is expressed in ΔCt values (ΔCt = $Ct_{reference} - Ct_{target}$). Relative changes in transcript levels compared with controls are expressed as $\Delta\Delta$Ct values ($\Delta\Delta$Ct = $\Delta Ct_{treated} - \Delta Ct_{control}$) as previously described[39].

Western blot analysis

Cells and tissues were harvested, lysed in RIPA buffer (Thermo Scientific) and supplemented with Halt Protease and Phosphatase Inhibitor Cocktail (Thermo Scientific). Protein extracts were subjected to centrifugation (6,000g) at 4°C and protein concentrations were determined using BCA assay (Pierce). Protein was separated on either NativePAGE™ Bis-Tris Gel System or 4-12 % SDS-Tris-Glycine Protein Gel. Separated proteins were transferred onto PDVF membranes (Invitrogen), and membranes were blocked with 5% non-fat dry milk in TBS and incubated with the indicated primary antibodies. After washing, membranes were incubated with appropriate secondary, HRP-linked antibodies (Pierce). Proteins were visualized by enhanced chemiluminescence and autoradiography (ECL; Amersham Biosciences, GE Healthcare).

Immunofluorescence analysis

Cells were plated on glass coverslips, treated with GI254023X (20 nM) or TGF-β as described, and fixed with 4% PFA for 10-15 min. The cells were then washed three times with PBS, blocked for one hour in blocking solution (10% goat serum; 0.1% triton-X in PBS) and incubated overnight at 4°C with a primary antibody against α-SMA (clone 1A4, Sigma-Aldrich; 1:100 in blocking solution). The next day, samples were washed three times with PBS and incubated for one hour with goat anti-mouse Alexa Fluor 488 and rhodamine phalloidin antibodies (Thermo Fisher Scientific) diluted 1:400 and 1:200, respectively, in blocking solution. Samples were washed three times with PBS and mounted with Vectashield antifade mounting medium with DAPI (Vectorlabs). Images were acquired with a Zeiss LSM780 confocal microscope (Zeiss).

Human plasma samples

Subjects with IPF were identified from those receiving care at the Massachusetts General Hospital. For study inclusion, IPF subjects had to satisfy IPF diagnostic criteria based on the 2011 recent joint consensus statement of the American Thoracic Society (ATS), European Respiratory Society (ERS), Japanese Respiratory Society[41], and Latin American Thoracic

Association[41] as determined by two investigators[41] (Supplementary Table 1). Partners Healthcare System Research Study Volunteer Program (RSVP) was used to recruit controls. Controls were at least 50 years of age, non-smokers, and without a history of chronic lung disease. Approval for plasma collection was obtained through the Partners Institutional Review Board. All subjects provided informed consent. Blood was obtained via venipuncture into tubes containing CTAD (citrate-theophylline-adenosine-dipyridamole). Whole blood was centrifuged at $1500\times$ g for 15 minutes to obtain plasma, which was then placed in aliquots and immediately frozen and stored at -80°C until analysis.

Human BAL samples

BAL samples from individuals with IPF and healthy volunteer donors was recovered after instillation of sterile 0.9% saline by flexible fiber-optic bronchoscopy. Bronchoscopies were preformed at both the Instituto Nacional de Enfermedades Respiratorias (INER), Mexico and the Massachusetts General Hospital (MGH), as previously described [38]. These studies were approved by the INER Ethics Committee and the MGH Institutional Review Board, and informed consent was obtained from all participants. BAL supernatants that were collected at MGH were immediately transferred to siliconized low-binding Eppendorf tubes, and supernatants from both institutions were kept at −70°C until use.

Statistical analysis

Sample sizes were determined by power analysis on the basis of our previous studies. In each experiment evaluating the effects of genetic depletion of ephrin-B2 in fibroblasts or ADAM10 inhibition on the extent of dermal and lung fibrosis produced in mice, n > or = 8 mice per group were used to account for the inherent variability in the fibrotic response of mice. Sample sizes were estimated based on an 80% power to detect a 50% reduction in the amount of fibrosis present in ephrin-b2 CKO mice or mice treated with ADAM10 inhibitor compared with wild-type control mice, accepting a Type I error rate of 0.05. No animals were excluded from analysis. Animals were distributed into groups of equal body weight and genotype before treatments. Experimental data were analyzed by unpaired Student's *t*-test for differences between each of the experimental conditions, two-way ANOVA for overall condition effects or log-rank test for differences in survival times using GraphPad Prism Software 5.0. The P values obtained are indicated in the Figures/Figure legends when statistically significant. *$P < 0.05$, **$P < 0.01$, ***$P < 0.001$ was considered significantly different between groups. All data displayed a normal distribution. Data are reported as mean ± SD.

Data availability

Data are available from the corresponding authors upon reasonable request. Life Sciences Reporting Summary is available online.

Supplementary Material

Refer to Web version on PubMed Central for supplementary material.

Acknowledgments

References

1. Ho YY, Lagares D, Tager AM, Kapoor M. Fibrosis--a lethal component of systemic sclerosis. Nat Rev Rheumatol. 2014; 10:390–402. [PubMed: 24752182]

2. Wynn TA, Ramalingam TR. Mechanisms of fibrosis: therapeutic translation for fibrotic disease. Nat Med. 2012; 18:1028–1040. [PubMed: 22772564]

3. Noble PW, Barkauskas CE, Jiang D. Pulmonary fibrosis: patterns and perpetrators. J Clin Invest. 2012; 122:2756–2762. [PubMed: 22850886]

4. Chambers RC, Mercer PF. Mechanisms of alveolar epithelial injury, repair, and fibrosis. Ann Am Thorac Soc. 2015; 12 Suppl 1:S16–20. [PubMed: 25830828]

5. Duffield JS. Cellular and molecular mechanisms in kidney fibrosis. J Clin Invest. 2014; 124:2299–2306. [PubMed: 24892703]

6. Selman M, et al. Accelerated variant of idiopathic pulmonary fibrosis: clinical behavior and gene expression pattern. PLoS One. 2007; 2:e482. [PubMed: 17534432]

7. Renzoni EA, et al. Gene expression profiling reveals novel TGFbeta targets in adult lung fibroblasts. Respir Res. 2004; 5:24. [PubMed: 15571627]

8. Parrinello S, et al. EphB signaling directs peripheral nerve regeneration through Sox2-dependent Schwann cell sorting. Cell. 2010; 143:145–155. [PubMed: 20869108]

9. Foo SS, et al. Ephrin-B2 controls cell motility and adhesion during blood-vessel-wall assembly. Cell. 2006; 124:161–173. [PubMed: 16413489]

10. Kullander K, Klein R. Mechanisms and functions of Eph and ephrin signalling. Nat Rev Mol Cell Biol. 2002; 3:475–486. [PubMed: 12094214]

11. Klein R. Eph/ephrin signalling during development. Development. 2012; 139:4105–4109. [PubMed: 23093422]

12. Noren NK, Lu M, Freeman AL, Koolpe M, Pasquale EB. Interplay between EphB4 on tumor cells and vascular ephrin-B2 regulates tumor growth. Proc Natl Acad Sci U S A. 2004; 101:5583–5588. [PubMed: 15067119]

13. Wang HU, Chen ZF, Anderson DJ. Molecular distinction and angiogenic interaction between embryonic arteries and veins revealed by ephrin-B2 and its receptor Eph-B4. Cell. 1998; 93:741–753. [PubMed: 9630219]

14. Kida Y, Ieronimakis N, Schrimpf C, Reyes M, Duffield JS. EphrinB2 reverse signaling protects against capillary rarefaction and fibrosis after kidney injury. J Am Soc Nephrol. 2013; 24:559–572. [PubMed: 23492730]

15. Avouac J, et al. Enhanced expression of ephrins and thrombospondins in the dermis of patients with early diffuse systemic sclerosis: potential contribution to perturbed angiogenesis and fibrosis. Rheumatology (Oxford). 2011; 50:1494–1504. [PubMed: 21454305]

16. Gerety SS, Wang HU, Chen ZF, Anderson DJ. Symmetrical mutant phenotypes of the receptor EphB4 and its specific transmembrane ligand ephrin-B2 in cardiovascular development. Mol Cell. 1999; 4:403–414. [PubMed: 10518221]

17. Luo H, et al. Efnb1 and Efnb2 proteins regulate thymocyte development, peripheral T cell differentiation, and antiviral immune responses and are essential for interleukin-6 (IL-6) signaling. J Biol Chem. 2011; 286:41135–41152. [PubMed: 21976681]

18. Astin JW, et al. Competition amongst Eph receptors regulates contact inhibition of locomotion and invasiveness in prostate cancer cells. Nat Cell Biol. 2010; 12:1194–1204. [PubMed: 21076414]

19. Lin KT, Sloniowski S, Ethell DW, Ethell IM. Ephrin-B2-induced cleavage of EphB2 receptor is mediated by matrix metalloproteinases to trigger cell repulsion. J Biol Chem. 2008; 283:28969–28979. [PubMed: 18713744]

20. Ji YJ, et al. EphrinB2 affects apical constriction in Xenopus embryos and is regulated by ADAM10 and flotillin-1. Nat Commun. 2014; 5:3516. [PubMed: 24662724]

21. Tomita T, Tanaka S, Morohashi Y, Iwatsubo T. Presenilin-dependent intramembrane cleavage of ephrin-B1. Mol Neurodegener. 2006; 1:2. [PubMed: 16930449]

22. Hattori M, Osterfield M, Flanagan JG. Regulated cleavage of a contact-mediated axon repellent. Science. 2000; 289:1360–1365. [PubMed: 10958785]

23. Lisle JE, et al. Murine, but not human, ephrin-B2 can be efficiently cleaved by the serine protease kallikrein-4: implications for xenograft models of human prostate cancer. Exp Cell Res. 2015; 333:136–146. [PubMed: 25724897]

24. Himanen JP, et al. Crystal structure of an Eph receptor-ephrin complex. Nature. 2001; 414:933–938. [PubMed: 11780069]

25. Pasquale EB. Eph-ephrin promiscuity is now crystal clear. Nat Neurosci. 2004; 7:417–418. [PubMed: 15114347]

26. Le Gall SM, et al. ADAMs 10 and 17 represent differentially regulated components of a general shedding machinery for membrane proteins such as transforming growth factor alpha, L-selectin, and tumor necrosis factor alpha. Mol Biol Cell. 2009; 20:1785–1794. [PubMed: 19158376]

27. Lagares D, et al. Endothelin 1 contributes to the effect of transforming growth factor beta1 on wound repair and skin fibrosis. Arthritis Rheum. 2010; 62:878–889. [PubMed: 20131241]

28. Border WA, Noble NA. Transforming growth factor beta in tissue fibrosis. N Engl J Med. 1994; 331:1286–1292. [PubMed: 7935686]

29. Ludwig A, et al. Metalloproteinase inhibitors for the disintegrin-like metalloproteinases ADAM10 and ADAM17 that differentially block constitutive and phorbol ester-inducible shedding of cell surface molecules. Comb Chem High Throughput Screen. 2005; 8:161–171. [PubMed: 15777180]

30. Janes PW, et al. Adam meets Eph: an ADAM substrate recognition module acts as a molecular switch for ephrin cleavage in trans. Cell. 2005; 123:291–304. [PubMed: 16239146]

31. Zhang K, Flanders KC, Phan SH. Cellular localization of transforming growth factor-beta expression in bleomycin-induced pulmonary fibrosis. Am J Pathol. 1995; 147:352–361. [PubMed: 7543734]

32. Munger JS, et al. The integrin alpha v beta 6 binds and activates latent TGF beta 1: a mechanism for regulating pulmonary inflammation and fibrosis. Cell. 1999; 96:319–328. [PubMed: 10025398]

33. Ramos C, et al. Fibroblasts from idiopathic pulmonary fibrosis and normal lungs differ in growth rate, apoptosis, and tissue inhibitor of metalloproteinases expression. Am J Respir Cell Mol Biol. 2001; 24:591–598. [PubMed: 11350829]

34. Tanaka M, Sasaki K, Kamata R, Sakai R. The C-terminus of ephrin-B1 regulates metalloproteinase secretion and invasion of cancer cells. J Cell Sci. 2007; 120:2179–2189. [PubMed: 17567680]

35. Selman M, Pardo A, Kaminski N. Idiopathic pulmonary fibrosis: aberrant recapitulation of developmental programs? PLoS Med. 2008; 5:e62. [PubMed: 18318599]

36. Selman M, Lopez-Otin C, Pardo A. Age-driven developmental drift in the pathogenesis of idiopathic pulmonary fibrosis. Eur Respir J. 2016; 48:538–552. [PubMed: 27390284]

37. Falivelli G, et al. Attenuation of eph receptor kinase activation in cancer cells by coexpressed ephrin ligands. PLoS One. 2013; 8:e81445. [PubMed: 24348920]

38. Tager AM, et al. The lysophosphatidic acid receptor LPA1 links pulmonary fibrosis to lung injury by mediating fibroblast recruitment and vascular leak. Nature medicine. 2008; 14:45–54.

39. Lagares D, et al. Inhibition of focal adhesion kinase prevents experimental lung fibrosis and myofibroblast formation. Arthritis and rheumatism. 2012; 64:1653–1664. [PubMed: 22492165]

40. Kapoor M, et al. Loss of peroxisome proliferator-activated receptor gamma in mouse fibroblasts results in increased susceptibility to bleomycin-induced skin fibrosis. Arthritis and rheumatism. 2009; 60:2822–2829. [PubMed: 19714649]

41. Raghu G, et al. An official ATS/ERS/JRS/ALAT statement: idiopathic pulmonary fibrosis: evidence-based guidelines for diagnosis and management. Am J Respir Crit Care Med. 2011; 183:788–824. [PubMed: 21471066]
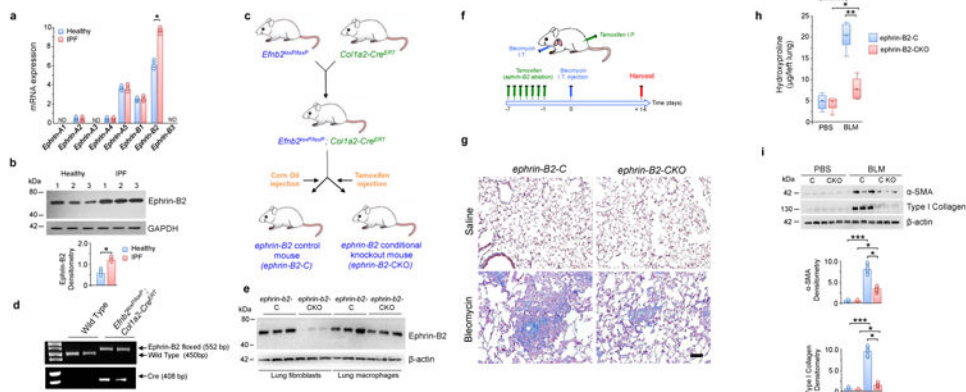
Figure 1.
Bleomycin-induced lung fibrosis is dependent on fibroblast ephrin-B2. (**a**) Gene expression of ephrin-A and -B ligands in human lung fibroblasts from healthy control donors (*n*=4) and individuals with idiopathic pulmonary fibrosis (n=4). mRNA expression was normalized to the level of GAPDH. (**b**) Ephrin-B2 protein levels in human fibroblasts from healthy controls (n=3) and individuals with IPF (n=3). GAPDH was used as a loading control for densitometry analysis. One representative out of two technical replicates is shown. (**c**) Schematic representation of the generation of *ephrinb2* conditional knockout (*ephrinb2*-CKO) mice. (**d**) Representative (n=30 mice per genotype) genotyping showing wild type mice (without Cre) and *Efnb2^{loxP/loxP}; Col1a2-Cre/ERT* mice: wild type band (450 bp), ephrin-B2 floxed band (552 base pairs (bp) and Creband (408 bp). (**e**) Representative Western blot of ephrin-B2 protein expression (normalized to β-actin) in lung fibroblasts and alveolar macrophages from *ephrinb2*-C and *ephrinb2*-CKO mice. n = 3 mice for all groups. One representative out of two technical replicates is shown. β-actin was used as a loading control. (**f,g**) Schematic diagram showing mice subjected to bleomycin-induced lung fibrosis model (f) and Masson's trichrome staining of lung sections from *ephrinb2*-C mice and *ephrinb2*-CKO mice 14 d after PBS or bleomycin challenge (**g**). Scale bar, 100 μm. Representative images are presented from n=8 mice per group per genotype. (**h**) Hydroxyproline content measured in the lungs of *ephrinb2*-C and *ephrinb2*-CKO mice at 14 d after bleomycin or PBS treatment. n= 6 for all groups. (**i**) Representative Western blot of α-SMA and collagen type I protein expression (normalized to β-actin) in total lung homogenates of *ephrinb2*-C and *ephrinb2*-CKO mice at 14 d after bleomycin (BLM) or PBS challenge. n =6 mice for all groups. One representative out of two technical replicates is shown. Data are presented as mean ± SD. *P< 0.05, Student's *t*-test (**a,b**). Data are presented as mean ± SD. *P < 0.05, **P < 0.01, two-way ANOVA. Center lines indicate median values, "+" denotes the mean, box edges indicate the 25th and 75th percentiles, and the whiskers extend to the most extreme data points (**h**). Data are presented as mean ± SD. *P < 0.05, ***P < 0.001, two-way ANOVA (**i**). Uncropped blot images are shown in Supplementary Figure 3.
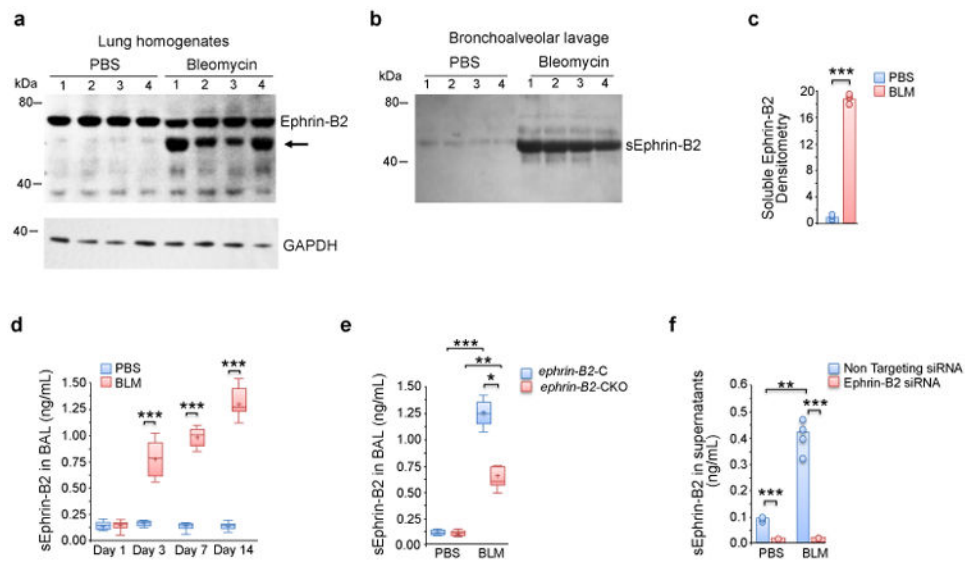
Figure 2.
Ephrin-B2 ectodomain is shed by fibroblasts upon lung injury. (**a**) Representative Western blot showing ephrin-B2 expression levels in total lung homogenates from 14 d PBS- and bleomycin-challenged C57BL/6N mice. n=4 mice for all groups. Arrow (←) indicates appearance of lower molecular weight band (~50 kDa). One representative out of two technical replicates is shown. (**b,c**) Representative Western blot showing cleaved soluble ephrin-B2 levels in BAL fluids from PBS- and bleomycin-challenged mice at day 14 after treatment (b) and its quantification of cleaved soluble ephrin-B2 protein (c). n=4 mice for all groups. One representative out of three technical replicates is shown. (**d**) Concentration of soluble ephrin-B2, as determined by ephrin-B2 ELISA, in BAL fluid from C57BL/6N mice at 1, 3, 7 and 14 d post-PBS- or bleomycin-challenge. n = 8 mice for all groups. (**e**) Concentration of ephrin-B2 in BAL fluids recovered from *ephrinb2*-C and *ephrinb2*-CKO mice at 14 d post-PBS or –bleomycin challenge. n = 5 mice for all groups. (**f**) Effect of ephrin-B2 siRNA *vs.* a non-targeting siRNA control on soluble ephrin-B2 generation by primary lung fibroblasts isolated from C57BL/6N mice 7 d post-PBS- or bleomycin-challenge. n = 5 for all groups. Data are presented as mean ± SD. ***P < 0.001, Student's *t*-test (**b,c,d**). Data are presented as mean ± SD. *P < 0.05, **P < 0.01, ***P < 0.001, two-way ANOVA (**e,f**). Uncropped blot images are shown in Supplementary Figure 4.
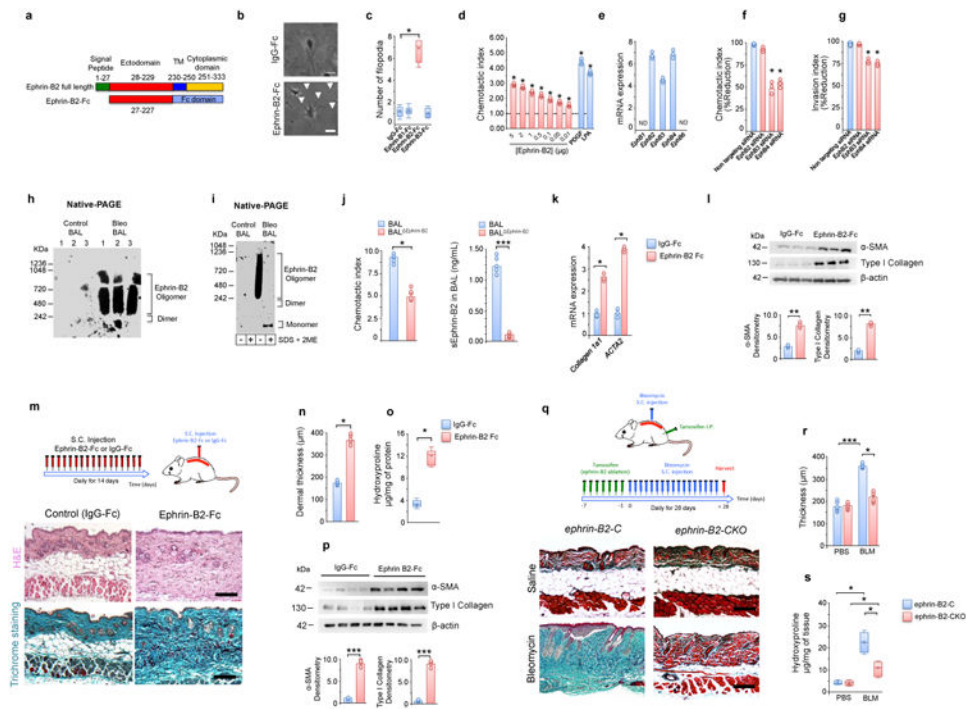
Figure 3.
Ephrin-B2 ectodomain directs fibroblast migration, invasion and myofibroblast differentiation *in vitro* and *in vivo*. (**a**) Domain structure of ephrin-B2 protein and recombinant ephrin-B2 ectodomain fused to Fc. (**b**) Representative phase contrast images showing the effect of pre-clustered ephrin-B2-Fc or IgG-Fc (control) treatment for 24 h on filopodia formation in primary human lung fibroblasts. Scale bars, 50 μm. n= 25-50 cells per condition. (**c**) Blinded quantitation of number of filopodia per cell upon IgG-Fc, ephrin-B1-Fc, ephrin-B2-Fc or ephrin-B3-Fctreatment. n= 25-50 cells per condition. (**d**) Chemotactic indices induced by ephrin-B2-Fc, lysophosphatidicacid (LPA) or platelet-derived growth factor-BB (PDGF-BB). Data are presented as fold increase over chemotaxis induced by IgG-Fc (dotted line). n = 4 for all groups. (**e**) Gene expression of *EphB* receptors (*EphB1*, *Ephb2*, *Ephb3*, *Ephb4* and *Ephb6*) in primary mouse lung fibroblasts. Gene expression was analyzed by quantitative RT-PCR (qPCR), mRNA expression was normalized to the level of GAPDH. n = 3 for all groups. (**f,g**) Effect of siRNA-mediated knockdown of EphB receptors on BAL-induced fibroblast chemotaxis and invasion. BAL from mice at day 7 post-bleomycin challenge was used as chemoattractant. n = 3 for all groups. *$P < 0.05$ versus non-targeting control siRNA, Student's *t*-test. (**h**) The oligomeric state of soluble ephrin-B2 from BAL samples from PBS- and bleomycin-challenged mice subjected to non-denaturing native gel electrophoresis. n = 3 for all groups. (**i**) Effect of SDS/2-β-mercaptoethanol on the formation of high molecular weight soluble ephrin-B2 oligomers in BAL. (**j**) Effect of soluble ephrin-B2 depletion by magnetic beads coated with anti-ephrin-B2 antibody on BAL-induced fibroblast chemotaxis of mouse lung fibroblasts. n = 5 for all groups. Data are presented as mean ± SD. *P < 0.05, ***P < 0.01, Student's *t*-test. (**k**) Effects of ephrin-B2-Fc or IgG-Fc on *collagen 1a1* and *ACTA2* mRNA expression by mouse lung fibroblasts. Data are presented as fold-increase over IgG-Fc-treated fibroblasts. (**l**) Effects of ephrin-B2-Fc or

IgG-Fc on α-SMA and collagen type Iprotein expression in mouse lung fibroblasts. Densitometry data (normalized by β-actin) is presented. n = 3 for all groups. (**m**) Schematic diagram (m, top) indicating that C57BL/6N mice were treated with daily subcutaneous injections of either pre-clustered ephrin-B2-Fc (n = 6) or IgG-Fc (n = 6) as control for 14 d. Results of Hematoxylin and Eosin and Masson's trichrome staining (m, bottom) for each treatment group. Scale bars, 100 μm.(**n,o,p**) Effects of ephrin-B2-Fc or IgG-Fc treatment on skin fibrosis as assessed by blinded analysis of dermal thickness of tissue sections (n, n = 5 for each treatment group), quantification of hydroxyproline content in skin biopsies (o, n = 6 for each treatment group) and Western blot showing α-SMA and collagen type I levels in skin (p,n = 4 for all groups). β-actin was used as a loading control for densitometry analysis. One representative out of two technical replicates is shown. Densitometry data is presented. (**q**) Schematic diagram (top) indicating that *ephrinb2*-C and *ephrinb2*-CKO mice were subjected to bleomycin-induced skin fibrosis model. Mice received daily subcutaneous injections of either PBS or bleomycin for 28 days. Representative images (bottom) of Masson's trichrome-stained skin of control *ephrinb2*-C and *ephrinb2*-CKO mice 28 d post-PBS or -bleomycin challenge. Scale bars, 100 μm. n = 6 for all groups. (**r**) Blinded analysis of dermal thickness of tissue sections from *ephrinb2*-C mice and *ephrinb2*-CKO mice 28 d after PBS or bleomycin challenge. n = 6 for all groups. (**s**) Hydroxyproline content in 6 mm skin biopsies from *ephrinb2*-C and *ephrinb2*-CKO mice treated with PBS or bleomycin. n = 6 for all groups. Data in are presented as mean ± SD. *$P < 0.05$, **$P < 0.01$, versus IgG-Fc treated fibroblasts. Student's *t*-test (c,d,j,k,l,n,o,p). (k). Data are presented as mean ± SD.*$P < 0.05$, two-way ANOVA (r,s). Uncropped blot images are shown in Supplementary Figure 5.
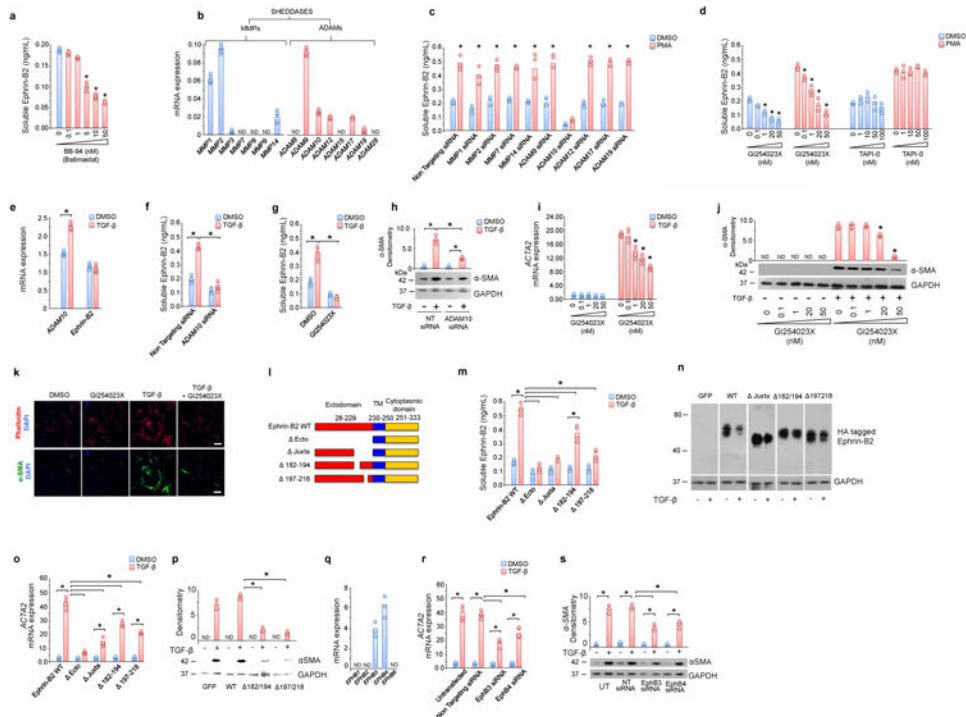
Figure 4.
ADAM10-mediated sEphrin-B2 generation is required for TGF-β1–induced myofibroblast differentiation. (**a**) Effect of BB-94 (Batimastat) treatment, a broad-spectrum inhibitor of both MMPs and ADAMs, on the generation of soluble ephrin-B2 in primary human lung fibroblasts. *$P < 0.05$ versus control (DMSO). (**b**) Gene expression of metalloproteinases (*MMPs* and *ADAMs*) in primary human lung fibroblasts. mRNA expression was normalized to the level of GAPDH. n = 5 sets of human lung fibroblasts analyzed. (**c**) Effect of siRNA-mediated knockdown of metalloproteinases on ephrin-B2 shedding by human lung fibroblasts. Concentration of ephrin-B2 in the conditioned media was determined by ELISA. Three sets of primary lung fibroblasts were used, n = 3 sets for all groups. *$P < 0.05$ versus control (DMSO). (**d**) Effect of GI254023X (ADAM10 inhibitor) and TAPI-0 (ADAM17 inhibitor) on constitutive and PMA-induced generation of soluble ephrin-B2 by primary human lung fibroblasts. Three sets of primary lung fibroblasts were used, n = 3 sets for all groups.. *$P < 0.05$ versus control (DMSO). (**e**) Gene expression of *ephrin-b2* and *ADAM10* in primary human lung fibroblasts treated with or without TGF-β (10 ng/mL) for 48 hours. GAPDH was used as housekeeping gene. *$P < 0.05$ versus TGF-β-treated fibroblasts. (**f**) Effect of siRNA-mediated knockdown of *ADAM10* on TGF-β–induced generation of soluble ephrin-B2 in human lung fibroblasts. Non-targeting siRNA was used as control. (**g**) Effect of ADAM10 inhibition with GI254023X (20 nM) on TGF-β–induced soluble ephrin-B2 generation in human lung fibroblasts. DMSO was used as control. n = 5 for all groups. (**h**) Effect of siRNA-mediated knockdown of *ADAM10* on TGF-β–induced α-SMA protein expression and densitometry (GAPDH used as a loading control) in human lung fibroblasts. Non-targeting siRNA was used as control. n = 4 for all groups. (**i**) Effect of ADAM10 inhibition with GI254023X (20 nM) on TGF-β–induced *ACTA2* gene expression in human lung fibroblasts. GAPDH was used as housekeeping gene. n = 4 for all groups. *$P < 0.05$

versus TGF-β-treated fibroblasts. (**j**) Effect of ADAM10 inhibition with GI254023X (20 nM) on TGF-β–induced α-SMA protein levels, with GAPDH as a loading control; n = 4 for all groups. *P < 0.05 versus TGF-β-treated fibroblasts. (**k**) Representative immunofluorescence images (n >6 images per condition) of human lung fibroblasts treated with vehicle (DMSO) or the ADAM10 inhibitor GI254023X (20 nM) and stained for α-SMA (green) to identify myofibroblasts, phalloidin (red) to visualize F-actin in fibroblasts and Hoechst 33342 (blue) to visualize nuclei. Scale bars, 50 μm. (**l**) Schematic diagram of ephrin-B2 wild type (WT) and ephrin-B2 mutants including ephrin-B2 [Ecto-HA], ephrin-B2 [Juxta-HA], ephrin-B2 [182-194-HA] and ephrin-B2 [197-218-HA]. (**m**) Effect of ephrin-B2 mutants on TGF-β-induced soluble ephrin-B2 generation in human lung fibroblasts as assessed by ephrin-B2 ELISA. n = 4 for all groups. (**n**) Effect of ephrin-B2 mutants on TGF-β-induced ephrin-B2 shedding in human lung fibroblasts as assessed by Western blot analysis of HA tagged ephrin-B2 WT and mutants. GAPDH as a loading control. (**o**) Effect of ephrin-B2 mutants on TGF-β–induced *ACTA2* gene expression in human lung fibroblasts. GAPDH was used as housekeeping gene. n = 4 for all groups. (**p**) Effect of ephrin-B2 mutants on TGF-β-induced *α-SMA* protein in human lung fibroblasts. GAPDH was used as a loading control. n = 3 for all groups. (**q**) Gene expression of EPHB receptors (*EPHB1*, *EPHB2*, *EPHB3*, *EPHB4* and *EPHB6*) in primary human lung fibroblasts. GAPDH was used as housekeeping gene. n = 3 for all groups. (**r**) Effect of siRNA-mediated knockdown of EphB receptors on TGF-β-induced *ACTA2* gene expression in human lung fibroblasts. GAPDH was used as housekeeping gene. n = 3 for all groups. (**s**) Effect of siRNA-mediated knockdown of EphB receptors on TGF-β-induced α-SMA protein levels, in human lung fibroblasts. GAPDH was used as loading control. n = 3 for all groups. All data in Fig. 4 are presented as mean ± SD. *P < 0.05, Student's t-test. Uncropped blot images are shown in Supplementary Figure 6.
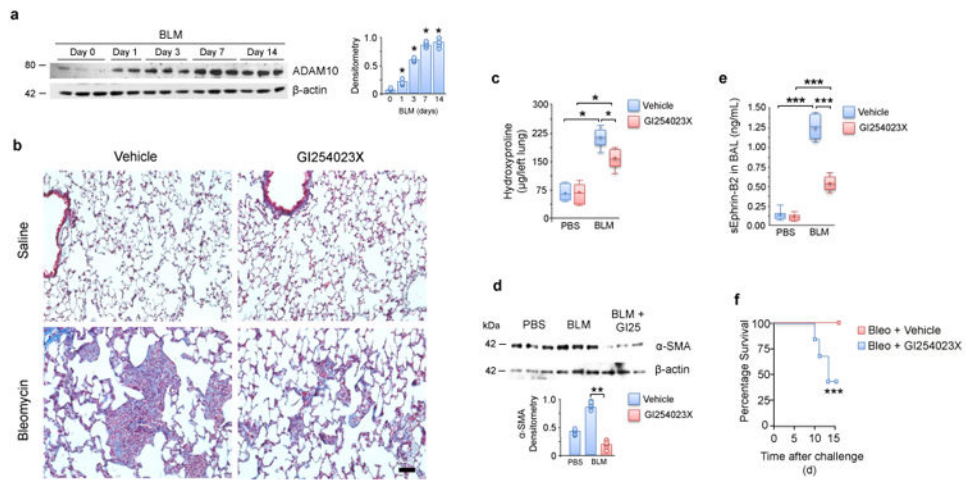
Figure 5.
ADAM10 inhibition prevents ephrin-B2 shedding, myofibroblast formation and lung fibrosis in mice. (**a**) Western blot (left) and densitometry (right) showing ADAM10 levels in lung homogenates after bleomycin challenge. β-actin was used as a loading control. n = 4 for all groups. Data are presented as mean ± SD. *$P < 0.05$ versus Day 0, Student's *t*-test. (**b**) Representative images (4 images from *n* = 10 mice per group) of Masson's Trichrome staining of lung sections from mice 14 d after PBS or bleomycin challenge and treated with ADAM10 inhibitor GI254023X or vehicle control. Scale bar, 100 μm. (**c**) Hydroxyproline content measured in the lungs of mice 14 d after bleomycin or PBS challenge treated with or without ADAM10 inhibitor GI254023X or vehicle control. N = 8 for all groups. (**d**) α-SMA protein expression by Western blot (top) and densitometry (bottom; normalized to β-actin) in total lung homogenates of mice 14 d after bleomycin or PBS challenge treated with or without ADAM10 inhibitor GI254023X or vehicle control. Representative blot shows 3 samples/group (n = 6 mice for all groups). (**e**) Concentration of soluble ephrin-B2 in BAL fluids recovered from mice at 14 d post-PBS or -bleomycin challenge treated with or without ADAM10 inhibitor GI254023X or vehicle control. n = 8 mice for all groups. (**f**) Survival curves for mice challenged with bleomycin and treated with or without ADAM10 inhibitor GI254023X or vehicle control. n = 10 mice per group. ***$P < 0.001$, log-rank test. Data are presented as mean ± SD. **$P < 0.01$, ***$P < 0.001$, two-way ANOVA (c,d,e). Uncropped blot images are shown in Supplementary Figure 7.
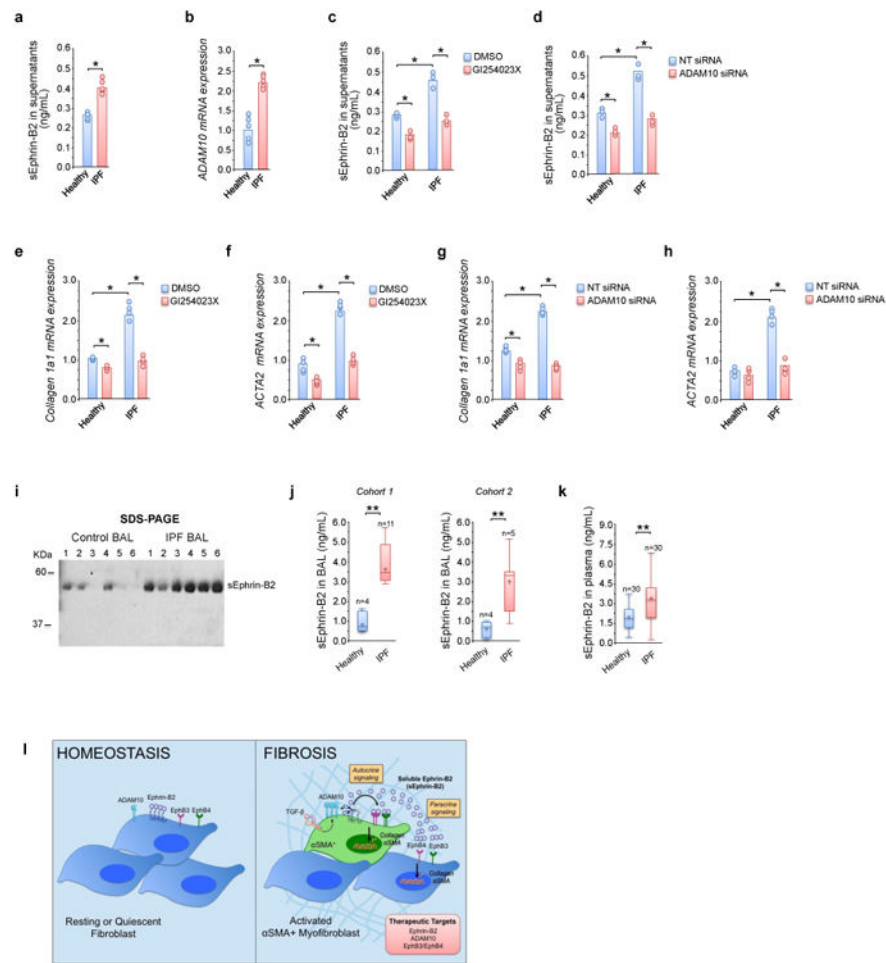
Figure 6.
ADAM10-mediated ephrin-B2 shedding in idiopathic pulmonary fibrosis. (**a**) Concentration of soluble ephrin-B2 in conditioned media from primary lung fibroblasts from control donors (n=5) and individuals with idiopathic pulmonary fibrosis (IPF; n=5), determined by ELISA. (**b**) *ADAM10* geneexpression in primary lung fibroblasts from donors (n=5) and individuals with IPF (n=5). mRNA expression was normalized to the level of GAPDH. (**c,d**) Effect of pharmacological inhibition of ADAM10 with GI254023X (20 nM) on soluble ephrin-B2 concentration in conditioned media. DMSO was used as vehicle control. n = 3 for all groups. (**d**) Effect of siRNA-mediated knockdown of *ADAM10* on soluble ephrin-B2 concentration in conditioned media. Non-targeting control siRNA was used as control. n = 3 for all groups. (**e,f**) Effect of pharmacological inhibition of ADAM10 with GI254023X (20 nM) on TGF-β–induced *collagen 1a1* (**e**) and *ACTA2* (**f**) expression in human lung fibroblasts *vs.* vehicle (DMSO) control. mRNA expression was normalized to the level of GAPDH. n = 4 for all groups. (**g,h**) Effect of siRNA-mediated knockdown of *ADAM10* on TGF-β–induced *collagen 1a1* and *ACTA2* expression in human lung fibroblasts. Non-targeting control siRNA was used as control. mRNA expression was normalized to the level of GAPDH. n = 4 for all groups. (**i**) Concentration of soluble ephrin-B2 in BAL fluid from control donors (n=6) and individuals with IPF (n=6) assessed by Western blotting. (**j**)

Concentration of soluble ephrin-B2 in BAL fluids from control donors (n=8) and individuals with IPF (n=16) assessed by ELISA. Data are stratified into two cohorts obtained from separate institutions. (**k**) Concentration of soluble ephrin-B2 in plasma from control donors (n=30) and individuals with IPF (n=30) assessed by ELISA. All data in Fig. 6 are presented as mean ± SD. $P < 0.05$, Student's t-test. Uncropped blot images are shown in Supplementary Figure 8. (**l**) Schematic diagram of the working model of ADAM10-mediated ephrin-B2 shedding in fibroblasts. Our results suggest that in fibroblasts during the development of fibrosis, soluble ephrin-B2 is produced by ADAM10 upregulation in TGF-β-stimulated fibroblasts. sEphrin-B2 then acts through EphB3/EphB4 receptors to further drive and/or amplify pro-fibrotic fibroblast effector functions, including migration, invasion, myofibroblast differentiation and extracellular matrix production in an autocrine and/or paracrine fashion.